Ramakrishna Mission Residential College (Autonomous)
Kolkata 700103, WB, India

Collaborative research in coordination chemistry of organic radicals

Number 4

Institute 1: Ramakrishna Mission Residential College (Autonomous)

Concerned Faculty: Dr. Prasanta Ghosh, Dept of Chemistry

&

Institute 2: **Max-Planck-Institut für Chemische Energiekonversion**

Stiftstrasse 34 - 36 / D - 45470 Mülheim an der Ruhr

Concerned Scientist: Dr Thomas Weyhermüller

Period of Investigation: 01-03-2014 to 31-12-2014

Project: Oxidovanadium Complexes of 2,2'-Bipyridine, 1,10 Phenanthroline, and *p*-Nitro-*o*-aminophenol

Output: The result was published in a journal of international repute

Publication: Oxidovanadium Complexes of 2,2'-Bipyridine, 1,10 Phenanthroline, and *p*-Nitro-*o*-aminophenol Radical versus Non-radical States

Madhusudan Shit, Sachinath Bera, Suvendu Maity, Subrata Maji, Thomas Weyhermüller and Prasanta Ghosh*
Eur. J. Inorg. Chem., 2016, *2016*, 330-338

Dr. Prasanta Ghosh

Dr Thomas Weyhermüller

ChemPubSoc Europe
DOI: 10.1002/ejic.201501246
EurJIC European Journal of Inorganic Chemistry
Full Paper

Oxidovanadium Complexes

Oxidovanadium Complexes of 2,2′-Bipyridine, 1,10 Phenanthroline, and *p*-Nitro-*o*-aminophenol – Radical versus Nonradical States

Madhusudan Shit,[a] Sachinath Bera,[a] Suvendu Maity,[a] Subrata Maji,[b] Thomas Weyhermüller,[c] and Prasanta Ghosh*[a]

Abstract: 2,2′-Bipyridine (bpy), 1,10-phenanthronline (phen) and *p*-nitro-*o*-aminophenol ($^{NO2}LH_2$) oxidovanadium complexes of the types $[(L_{ONO}^{2-})(VO)(bpy)]$ (**1**), $[(L_{ONO}^{2-})(VO)(phen)]$ (**2**) and $[(L_{ONO}^{2-})(VO)(^{NO2}L_{ISQ}^{\bullet-})][NHEt_3]$ (**3**$^-$ $NHEt_3^+$; $^{NO2}L_{ISQ}^{\bullet-}$ = *p*-nitro-*o*-iminobenzosemiquinonate radical) were isolated with (*E*)-2-(3-hydroxy-3-phenyltriaz-1-en-1-yl)benzoic acid ($L_{ONO}H_2$) as a co-ligand. The single-crystal X-ray bond parameters and electron paramagnetic resonance (EPR) spectra authenticated that **1** and **2** are the oxidovanadium(IV) complexes of bpy and phen, whereas **3**$^-$ is the $^{NO2}L_{ISQ}^{\bullet-}$ complex of oxidovanadium(IV) and undergoes reversible one-electron oxidation and reduction at lower potentials. Density functional theory (DFT) calculations established that the closed-shell-singlet (CSS) solution of **3**$^-$ is unstable owing to open-shell-singlet (OSS) perturbation. The CSS → OSS charge-transfer transition that appears at λ = 632 nm is absent for **1** and **2**. Complex **3** is a hybrid of the $[(L_{ONO}^{2-})(VO^{2+})(^{NO2}L_{IQ})]$ ($^{NO2}L_{IQ}$ = *p*-nitro-*o*-iminobenzoquinone) and $[(L_{ONO}^{2-})(VO^{3+})(^{NO2}L_{ISQ}^{\bullet-})]$ states, whereas **3**$^{2-}$ is an oxidovanadium(IV) complex of the type $[(L_{ONO}^{2-})(VO^{2+})(^{NO2}L_{AP}^{2-})]^{2-}$ ($^{NO2}L_{AP}^{2-}$ = *p*-nitro-*o*-amidophenolato).

Introduction

The bioactive oxidovanadium core ($VO^{2+/3+}$) is redox-noninnocent and participates in electron-transfer reactions at low potential. The roles of oxidovanadium ions in the activities of the haloperoxidases[1] and vanadium nitrogenase[2] are established. The importance of oxidovanadium ions to the alleviation of diabetes mellitus symptoms[3] and to the inhibition of several phosphate-metabolizing enzymes[4] has been recognized in several research articles. This has fostered the development of the coordination chemistry of vanadium with medicinal importance.[5] In this context, the coordination complexes of the oxidovanadium ion with organic radicals that participate in electron-transfer reactions at relatively low potentials are significant. The oxidovanadium complexes are numerous;[6] however, oxidovanadium complexes of organic radicals are limited.[7] In this project, we wanted to develop oxidovanadium complexes that were likely to be involved in multi-electron-transfer reactions. The oxidovanadium complexes of redox-noninnocent ligands are designed to furnish electron counter centres other than the $VO^{2+/3+}$ core. The redox-noninnocent ligands that we used in this particular work are heterocyclic diimines, 2,2′-bipyridine (bpy), 1,10-phenanthronline (phen) and *p*-nitro-*o*-aminophenol ($^{NO2}LH_2$). The bpy and phen ligands are electron acceptors and afford $bpy^{\bullet-}$ and $phen^{\bullet-}$ anion radicals,[8] whereas $^{NO2}LH_2$ is a two-electron reducing agent as depicted in Scheme 1.[9] The coordination of $^{NO2}LH_2$ to the redox-active oxidovanadium ion can afford several tautomeric electronic states, as listed in Table 1. In this work, we isolated an oxidovanadium complex that contains the (–1, +4) state.

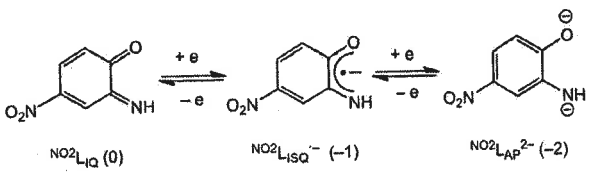

$^{NO2}L_{IQ}$ (0) $^{NO2}L_{ISQ}^{\bullet-}$ (–1) $^{NO2}L_{AP}^{2-}$ (–2)

Scheme 1. Three different oxidation states of $^{NO2}LH_2$ with charges in parentheses.

Table 1. Electronic states of the oxidovanadium complexes with $^{NO2}LH_2$ (charge of the ligand, redox state of the vanadium ion) and the total spin state.

Electronic state	Spin state	Type
(–2, +5)	$S = 0$	I
(–2, +4)	$S = 1/2$	II
(–1, +4)	$S = 0$ or 1	III
(–1, +5)	$S = 1/2$	IV
(0, +4)	$S = 1/2$	V
(0, +5)	$S = 0$	VI
(–2, +3)	$S = 1$	VII

[a] Department of Chemistry, R. K. Mission Residential College, Narendrapur, Kolkata 700103, India
E-mail: ghosh@pghosh.in
http://www.pghosh.in
[b] Department of Chemistry, Bangabasi College, No.19, Rajkumar Chakraborty Sarani, Baithakkhana, Kolkata 700009, India
[c] Max-Planck-Institut für Chemische Energiekonversion, Stiftstrasse 34–36, 45470 Mülheim an der Ruhr, Germany
Supporting information for this article is available on the WWW under http://dx.doi.org/10.1002/ejic.201501246.

The oxidovanadium(IV) complexes of types [(L_{ONO}^{2-})-(VO)(bpy)] (**1**), [(L_{ONO}^{2-})(VO)(phen)] (**2**) and [(L_{ONO}^{2-})-(VO)($^{NO2}L_{ISQ}^{\bullet-}$)][$NHEt_3$] (**3**$^-$ $NHEt_3^+$) reported in this work are summarized in Figure 1 ($^{NO2}L_{ISQ}^{\bullet-}$ = *p*-nitro-*o*-iminobenzosemiquinone radical). The dianionic tridentate azoxybenzoic acid derivative (*E*)-2-(3-hydroxy-3-phenyltriaz-1-en-1-yl)benzoic acid ($L_{ONO}H_2$) was used as a redox-innocent coligand. Complexes **1** and **2** are paramagnetic, whereas complex **3**$^-$ $NHEt_3^+$ is a strongly coupled *o*-iminobenzosemiquinonate anion radical ($L_{ISQ}^{\bullet-}$) complex of oxidovanadium(IV) and diamagnetic. In cyclic voltammetry, the cathodic and anodic redox peaks of **1** and **2** are both irreversible, whereas **3**$^-$ $NHEt_3^+$ exhibits reversible cathodic and anodic waves at relatively lower potentials. In this article, the syntheses, spectra and single-crystal X-ray structures of **1**, **2** and **3**$^-$ $NHEt_3^+$ are reported. The electronic structures of the complexes were elucidated by electron paramagnetic resonance (EPR) spectroscopy and density functional theory (DFT) calculations. The members of the electron-transfer series of the **3**$^-$ ion were investigated by spectroelectrochemical measurements, EPR spectroscopy and unrestricted DFT calculations.

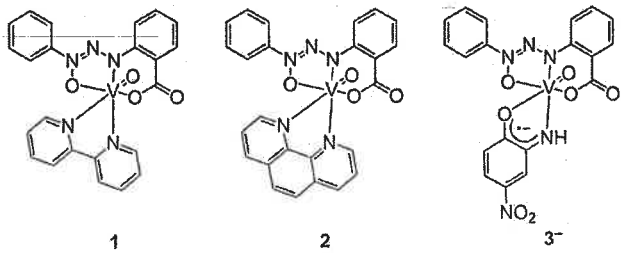

Figure 1. Isolated oxidovanadium complexes.

Results and Discussion

Syntheses

Complexes **1** and **2** were isolated from the reactions of $VO(acac)_2$ (acac = acetylacetonate) with bpy and phen in the presence of the tridentate benzoic acid derivative $L_{ONO}H_2$ in boiling methanol in air. The similar reaction of $VO(acac)_2$ with $^{NO2}LH_2$ in the presence of triethylamine afforded **3**$^-$ $NHEt_3^+$. The complexes were substantiated by elemental analysis, mass spectrometry and IR spectroscopy. In the IR spectra, the V=O stretching vibrations of **1**, **2** and **3**$^-$ $NHEt_3^+$ appear at $\tilde{\nu}$ = 964, 966 and 944 cm^{-1}, respectively. The ^1H and ^{51}V NMR spectra of **3**$^-$ $NHEt_3^+$ were recorded, and the relevant data are listed in the Experimental Section.

Single-Crystal X-ray Structures

The molecular geometries of the crystalline complexes were authenticated by single-crystal X-ray structure determinations of **1**·H_2O, **2**·H_2O and **3**$^-$ $NHEt_3^+$. The molecular geometries of **1**·H_2O and **2**·H_2O are shown in Figure 2, and the bond parameters are summarized in Table 2. Complexes **1**·H_2O and **2**·H_2O crystallize in the $P2_1/c$ space group. The V^{IV}=O bond lengths are 1.602(5) and 1.602(2) Å, and the V^{IV}–$O_{carboxylato}$ bond lengths in **1**·H_2O and **2**·H_2O are 1.976(5) and 1.962(2) Å, respectively. The V^{IV}–$O_{N\text{-}oxide}$ bond lengths are 1.982(5) and 1.976(2) Å, and the V^{IV}–N_{azo} bond lengths are 2.022(6) and 2.027(2) Å, respectively. The V^{IV}–N_{bpy} bond length [2.307(6) Å] *trans* to the V=O bond is somewhat longer than the V^{IV}–N_{bpy} bond length [2.168(6) Å]

Table 2. Selected experimental bond lengths [Å] of **1**·H_2O and **2**·H_2O and corresponding calculated parameters.

Bond	**1**·H_2O	**2**·H_2O
V–O(1)	1.976(5)	1.9616(16)
V–N(10)	2.022(6)	2.0270(18)
V–O(19)	1.982(5)	1.9763(15)
V–N(21)	2.307(6)	2.3465(19)
V–N(32)	2.168(6)	2.1474(18)
V–O(40)	1.602(5)	1.6020(16)
C(2)–O(1)	1.295(10)	1.284(3)
C(2)–O(3)	1.226(11)	1.244(3)
C(2)–C(4)	1.495(11)	1.502(3)
C(4)–C(9)	1.396(10)	1.412(3)
C(9)–N(10)	1.431(9)	1.421(3)
N(10)–N(11)	1.339(8)	1.332(2)
N(11)–N(12)	1.287(8)	1.286(2)

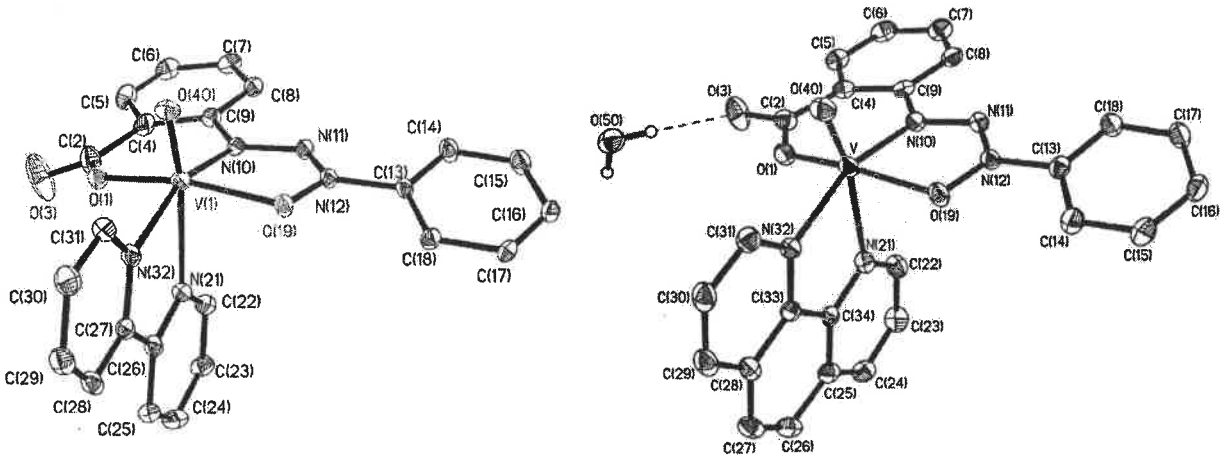

Figure 2. Molecular geometries of **1**·H_2O and **2**·H_2O (40 % ellipsoids; H atoms are omitted for clarity).

trans to the V–$N_{triazene}$ bond owing to the stronger *trans* effect of the V=O bond. The corresponding V^{IV}–N_{phen} bond lengths in **2**·H_2O are 2.346(5) and 2.147(5) Å, respectively.

The V–N_{bpy} and V–N_{phen} bond lengths correlate well to those reported for other oxidovanadium(IV) complexes of bpy and phen.[10] The two different N–N bond lengths in **1**·H_2O of 1.339(8) and 1.287(8) Å correspond to the Ar–$N^+(O^-)$=N–N^-–Ar–COO^- description of the L_{ONO}^{2-} ligand. The corresponding N–N bond lengths in **2**·H_2O are 1.332(2) and 1.286(2) Å. The C–O bond lengths of the carboxylato function in **1**·H_2O are 1.295(10) and 1.226(11) Å, whereas these are 1.284(3) and 1.244(3) Å in **2**·H_2O.

Complex **3**$^-$ $NHEt_3^+$ crystallizes in the $P\bar{1}$ space group. The molecular geometry is illustrated in Figure 3, and the bond parameters are summarized in Table 3. The V=O bond length is 1.608(2) Å. The V–$O_{carboxylato}$, V–$O_{N\text{-}oxide}$ and V–N_{azo} bond lengths are 1.941(2), 1.971(2) and 2.053(2) Å, respectively. The X-ray bond parameters are significant for the analysis of the redox state of the $^{NO2}L^{2-}$ ligand in crystalline **3**$^-$ $NHEt_3^+$. The C–O and C–N bond lengths of 1.283(3) and 1.358(3) Å, respectively, are relatively short and correlate well to those reported for *o*-iminobenzosemiquinonate anion radicals coordinated to oxidovanadium(IV) ions[7] and other transition-metal ions.[11] In addition, the quinoidal distortion of the C–C bond lengths of the phenyl ring [C22–C23 1.367(4) and C24–C25 1.379(4) Å] is consistent with the oxidation of $^{NO2}LH_2$ to $^{NO2}L_{ISQ}^{\bullet-}$ in the **3**$^-$ ion. The V–$O_{carboxylato}$, V–$O_{N\text{-}oxide}$ and V–$N_{triazene}$ bond lengths are similar to those found in **1**·H_2O and **2**·H_2O. Thus, the **3**$^-$ ion is an oxidovanadium(IV) complex of the *o*-iminobenzosemiquinone anion radical ($^{NO2}L_{ISQ}^{\bullet-}$). The V–N_{ISQ} bond length of 1.907(2) Å is relatively short, maybe as a result of the coupling of the unpaired electron of the oxidovanadium(IV) ion to the $^{NO2}L_{ISQ}^{\bullet-}$ radical anion. The V–O_{ISQ} bond length of 2.199(2) Å is longer because of the *trans* effect of the V=O bond, as observed for **1**·H_2O and **2**·H_2O, in which the V^{IV}–N_{bpy} and V^{IV}–N_{phen} bonds *trans* to the V=O bonds are longer (Table 2). Moreover, owing to the localization of spin to the –NH function, the resonance forms (Scheme 3) with the weak C=O donor dominate and the V–O_{ISQ} bond becomes longer.

Table 3. Selected experimental bond lengths [Å] of **3**$^-$ $NHEt_3^+$ and the corresponding calculated parameters of **3**$^-$, **3** and **3**$^{2-}$.

Bond	Experimental	OSS (calcd.)		
	3$^-$ $NHEt_3^+$	**3**$^-$	**3**	**3**$^{2-}$
V(1)–O(1)	1.941(2)	1.888	1.817	1.995
V(1)–N(10)	2.053(2)	2.122	2.066	2.112
V(1)–O(19)	1.971(2)	2.008	1.957	2.106
V(1)–N(27)	1.907(2)	1.886	1.974	2.014
V(1)–O(20)	2.199(2)	2.239	2.356	2.267
V(1)–O(40)	1.608(2)	1.587	1.574	1.603
C(2)–O(1)	1.284(3)	1.305	1.333	1.282
C(2)–O(3)	1.236(3)	1.230	1.217	1.245
C(2)–C(4)	1.497(3)	1.513	1.499	1.534
C(4)–C(9)	1.403(4)	1.415	1.413	1.421
C(9)–N(10)	1.415(3)	1.410	1.417	1.403
N(10)–N(11)	1.310(3)	1.302	1.302	1.304
N(11)–N(12)	1.282(3)	1.287	1.281	1.299
N(12)–O(19)	1.330(3)	1.331	1.334	1.321
O(20)–C(21)	1.283(3)	1.278	1.256	1.282
C(21)–C(26)	1.441(3)	1.449	1.477	1.465
C(26)–N(27)	1.358(3)	1.373	1.334	1.360
C(21)–C(22)	1.414(4)	1.427	1.441	1.427
C(22)–C(23)	1.367(4)	1.382	1.368	1.386
C(23)–C(24)	1.403(4)	1.414	1.431	1412
C(24)–C(25)	1.379(4)	1.405	1.377	1.423
C(25)–C(26)	1.387(4)	1.391	1.418	1.396

^{51}V NMR Spectroscopy

^{51}V NMR spectroscopy is an important tool for the elucidation of the electronic states of oxidovanadium complexes containing redox-noninnocent ligands.[12] The ^{51}V resonance signal of **3**$^-$ $NHEt_3^+$ in $CDCl_3$ is deshielded to δ = –13.24 ppm, as shown in Figure 4. This chemical shift correlates well to those of the oxidovanadium(IV) ion coupled to *o*-benzosemiquinonate and *o*-iminobenzosemiquinonate anion radicals[7b] and supports the existence of a coupled $V^{IV}O(^{NO2}L_{ISQ}^{\bullet-})$ state in the **3**$^-$ ion.

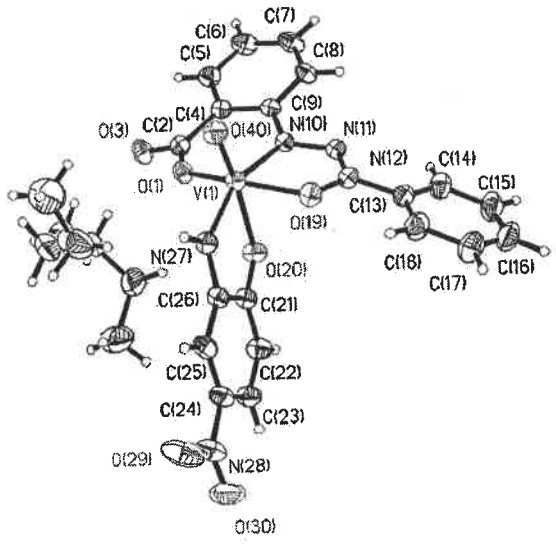

Figure 3. Molecular geometry of crystalline **3**$^-$ $NHEt_3^+$ (40 % ellipsoids).

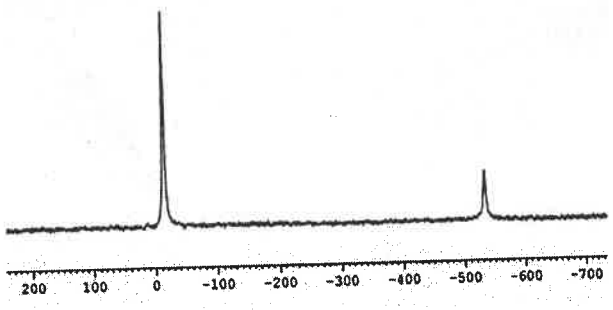

Figure 4. ^{51}V NMR spectrum of the **3**$^-$ ion in $CDCl_3$ illustrating the chemical shift [ppm] with respect to that of a vanadate salt (δ = –524.4 ppm).

Redox Series

The redox activities of **1**, **2** and **3**$^-$ in CH_2Cl_2 at 298 K were investigated by cyclic voltammetry. The cyclic voltammograms

are shown in Figure 5, and the redox potential data referenced to the ferrocenium/ferrocene couple are summarized in Table 4. The cathodic waves of **1** and **2** owing to the bpy/bpy$^{\bullet-}$ or phen/phen$^{\bullet-}$ couples are irreversible, whereas the anodic and cathodic waves of **3**$^-$ at 0.33 and −1.02 V for the $^{NO2}L_{IQ}{}^0/^{NO2}L_{ISQ}{}^{\bullet-}$ and $^{NO2}L_{ISQ}{}^{\bullet-}/^{NO2}L_{AP}{}^{2-}$ ($^{NO2}L_{AP}{}^{2-}$ = *p*-nitro-*o*-amidophenolato) couples are quite reversible, as depicted in Figure 5 (c). Complex **1** reveals an anodic wave at 0.70 V, for which the peak-to-peak separation is relatively high.

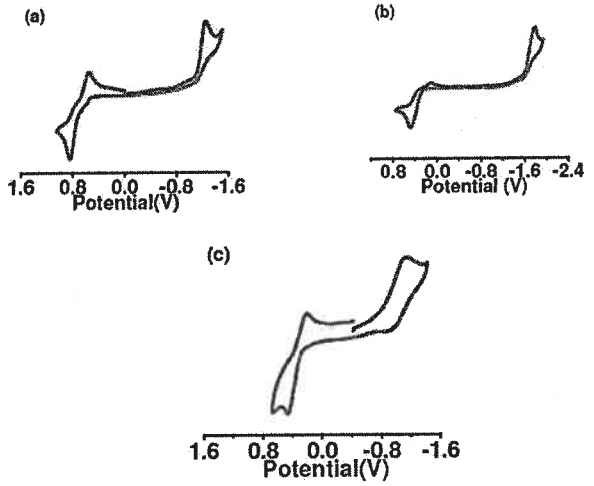

Figure 5. Cyclic voltammograms of (a) **1**, (b) **2** and (c) **3**$^-$ in CH_2Cl_2 {0.20 M $[N(nBu)_4]PF_6$} at 298 K.

Table 4. Redox potential data of **1**, **2** and **3**$^-$ $NHEt_3{}^+$ determined by cyclic voltammetry in CH_2Cl_2.

	$E_{1/2}{}^1$ [V] (ΔE, mV)[a]	$E_{1/2}{}^2$ [V] (ΔE, mV)[a]
1	0.70 (300)	−1.24[c]
2	0.48[b]	−1.78[c]
3$^-$ $NHEt_3{}^+$	0.33 (230)	−1.02 (190)

[a] Peak-to-peak separation in mV. [b] Anodic peak. [c] Cathodic peak.

The electrochemically generated **3** and **3**$^{2-}$ ion were further investigated by spectroelectrochemical measurements and broken-symmetry DFT calculations. The one-electron oxidation of **3**$^-$ affords a *p*-nitro-*o*-iminobenzoquinone ($^{NO2}L_{IQ}$) complex of the type $[(L_{ONO}{}^{2-})(VO^{2+})(^{NO2}L_{IQ})]$ (**3**), whereas the one-electron reduction of **3**$^-$ produces a *p*-nitro-*o*-amidophenolato complex of the type $[(L_{ONO}{}^{2-})(VO^{3+})(^{NO2}L_{AP}{}^{2-})]^-$ (**3**$^{2-}$), as depicted in Scheme 2.

$$(0, +4) \underset{-e}{\overset{+e}{\rightleftharpoons}} (-1, +4) \underset{-e}{\overset{+e}{\rightleftharpoons}} (-2, +4)$$

3 **3**$^-$ **3**$^{2-}$

Scheme 2. Redox series of the **3**$^-$ ion.

EPR Spectroscopy

The X-band EPR spectra of **1**, **2** and the electrochemically generated **3** and **3**$^{2-}$ ions were recorded in CH_2Cl_2 at 298 K. The spectra are illustrated in Figure 6, and the simulated *g* parameters and coupling constants are summarized in Table 5. Complexes **1** and **2** exhibit hyperfine EPR spectra owing to the ^{51}V (I = 7/2) nucleus, and the simulated *g* values are 1.965, which is consistent with the existence of oxidovanadium(IV) ions in **1** and **2**. The hyperfine EPR spectra of **3** and the **3**$^{2-}$ ion in CH_2Cl_2 are similar to those of **1** and **2**, and the simulated *g* values of 1.962 and 1.966, respectively, authenticate that **3** and **3**$^{2-}$ ions are the oxidovanadium(IV) complexes of types $[(L_{ONO})(VO)(^{NO2}L_{IQ}{}^0)]$ (0, +4) and $[(L_{ONO})(VO)(^{NO2}L_{AP}{}^{2-})]^{2-}$ (−2, +4), as depicted in Scheme 2.

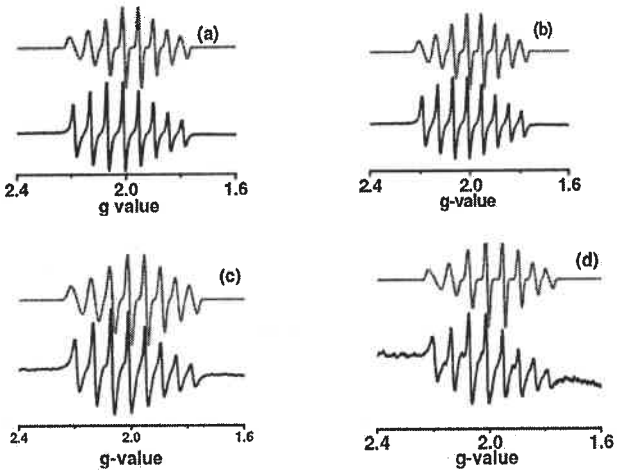

Figure 6. X-band EPR spectra of (a) **1**, (b) **2**, (c) **3** and (d) **3**$^{2-}$ in CH_2Cl_2 solution at 298 K (black, experimental; red, simulated).

Table 5. X-band EPR spectral parameters of **1**, **2**, **3** and **3**$^{2-}$ ions in CH_2Cl_2 at 298 K.

	g	*A* [G]	Line width
1	1.965	90 (^{51}V, I = 7/2)	2.1
2	1.965	90 (^{51}V, I = 7/2)	2.2
3	1.962	92 (^{51}V, I = 7/2)	2.5
3^{2-}	1.966	91 (^{51}V, I = 7/2)	1.8

DFT Calculations

The gas-phase geometry of **3**$^-$ was optimized for the singlet spin state at the B3LYP level of theory. The calculated bond parameters are listed in Table 3. The bond parameters correlate well to those obtained from the single-crystal X-ray structure determination of **3**$^-$ $NHEt_3{}^+$. Analyses of the molecular orbitals authenticated that the highest occupied molecular orbital (HOMO) of **3**$^-$ is constituted of both vanadium d orbitals and $L_{ONO}{}^{2-}$ ligand orbitals as shown in Figure 7, and the closed-shell-singlet (CSS) solution of **3**$^-$ is unstable owing to the closed-shell-singlet (CSS) → open-shell-singlet (OSS) perturbation. This suggests a possibility that the lowest-energy wave function is a singlet diradical instead of a closed-shell singlet and requires an unrestricted broken-symmetry (BS) solution for

a proper description. To solve this issue, the unstable CSS solution of $\mathbf{3}^-$ was reoptimized with an open-shell-singlet (OSS) state, which authenticates the diradical character of the $\mathbf{3}^-$ ion. The energy of the OSS solution is 0.34 kJ/mol lower than that of the CSS solution. The bond parameters of the OSS solution are listed in Table 3. The calculated C–N and C–O lengths of the chelate are 1.373 and 1.278 Å, respectively. The calculated amount of α spin localized on the vanadium ion is 34 %, which correlates to a significant oxidovanadium(IV) contribution in the $\mathbf{3}^-$ ion. A plot of the atomic spin densities is depicted in Figure 8. The dominant localization of the β spin on the coordinated N atom supports the resonance forms B and C (Scheme 3).

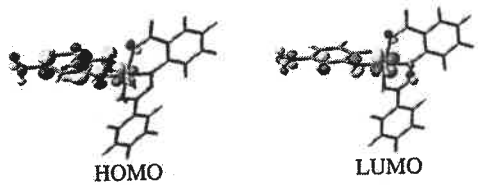

Figure 7. Frontier molecular orbitals of the $\mathbf{3}^-$ ion.

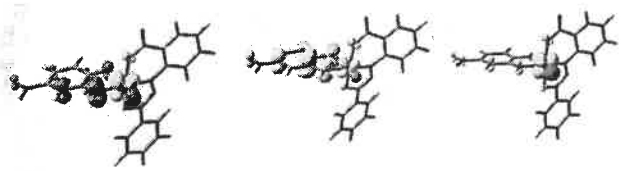

Figure 8. Atomic spin density plots of (a) $\mathbf{3}^-$, (b) **3** and (c) $\mathbf{3}^{2-}$ obtained from OSS calculations [Mulliken spin densities: $\mathbf{3}^-$: V 0.33, O(20) –0.03, N(27) –0.16; **3**: V 0.19, O(20) 0.19, N(27) 0.15; $\mathbf{3}^{2-}$: V 1.08, O(20) –0.02, N(27) 0.02].

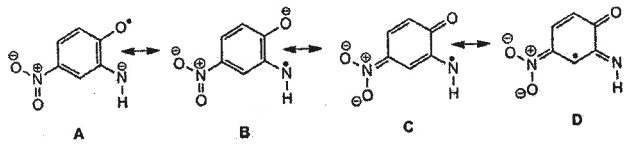

Scheme 3. Resonance structures of $^{NO2}L_{ISQ}^{\bullet-}$.

The average C–O/N bond lengths of 1.321 Å are consistent with those of the *o*-iminobenzosemiquinone anion radicals coordinated to transition-metal ions.[7b–7d,9] Thus, the DFT calculations and X-ray bond parameters suggest a contribution of the (–1, +4) state (Table 1) to the ground electronic state of the $\mathbf{3}^-$ ion, which is defined as a hybrid of the $[(L_{ONO}^{2-})(VO^{2+})(^{NO2}L_{ISQ}^{\bullet-})]^-$ (–1, +4) and $[(L_{ONO}^{2-})(VO^{3+})(^{NO2}L_{AP}^{2-})]^-$ (–2, +5) states.

The gas-phase geometries of **3** and $\mathbf{3}^{2-}$ were optimized with doublet spin states. The calculated bond parameters are summarized in Table 3. The calculated C–N and C–O bond lengths of the aminophenol ligand of **3** of 1.334 and 1.256 Å, respectively, are somewhat shorter than those of $\mathbf{3}^-$ and are consistent with those of the *o*-iminobenzoquinone state, $^{NO2}L_{IQ}^{0}$, of the ligand. A plot of the atomic spin densities of **3** is shown in Figure 8 and authenticates the delocalization of the spin density over the vanadium ion and aminophenol ligand. The localization of spin density on the vanadium ion signifies the existence of an oxidovanadium(IV) ion, whereas the spin density on the redox-active aminophenol ligand signifies the existence of a $^{NO2}L_{ISQ}^{\bullet-}$ radical anion coordinated to the oxidovanadium(V) in **3**. Thus, the ground electronic state of **3** is defined by a hybrid of $[(L_{ONO}^{2-})(VO^{2+})(^{NO2}L_{IQ})]$ (0, +4) and $[(L_{ONO}^{2-})(VO^{3+})(^{NO2}L_{ISQ}^{\bullet-})]$ (–1, +5) states.

The calculated C–N and C–O bond lengths of the aminophenol fragments of the $\mathbf{3}^{2-}$ ion are 1.359 and 1.282 Å. The atomic spin density, as depicted in Figure 8, is completely localized on the vanadium ion and correlates to the existence of the diamagnetic $^{NO2}L_{AP}^{2-}$ coordinated to the oxidovanadium (IV) ion in the $\mathbf{3}^{2-}$ ion. The somewhat shorter average C–O/N bond lengths are the effect of the participation of the phenolato and amido functions in resonance with the $-NO_2$ group, as shown in Scheme 4.

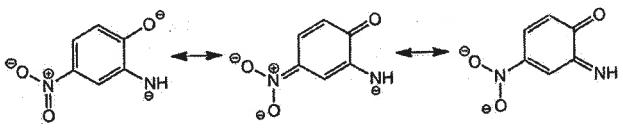

Scheme 4. Resonance structures of $^{NO2}L_{AP}^{2-}$.

The effect of resonance with the $-NO_2$ group is largest for the $\mathbf{3}^{2-}$ ion, which exhibits the shortest C–NO_2 bond length, and the effect is the smallest for **3**. The C–NO_2 bond length [Å] follows the order 1.412 ($\mathbf{3}^{2-}$) < 1.433 ($\mathbf{3}^-$) < 1.468 (**3**). Thus, on the basis of the atomic spin density distribution and the EPR spectrum, the $[(L_{ONO}^{2-})(VO^{2+})(^{NO2}L_{AP}^{2-})]^{2-}$ state (–2, +4) is assigned to the ground electronic state of the $\mathbf{3}^{2-}$ ion.

The electronic state of the $\mathbf{1}^+$ ion was established by DFT calculations. The gas-phase geometry of the $\mathbf{1}^+$ ion was optimized with a singlet spin state. In the $\mathbf{1}^+$ ion, the V–$O_{carboxylate}$, V–O_{azoxy}, V–N_{azoxy} and V=O lengths are shorter than those of the $\mathbf{3}^-$ ion. The V–$O_{carboxylate}$ and V–O_{azoxy} bond lengths are 1.796 and 1.944 Å, whereas those of the $\mathbf{3}^-$ ion are 1.888 and 2.008 Å, respectively. The V–N_{azoxy} and V=O bond lengths of the $\mathbf{1}^+$ ion are 2.028 and 1.577 Å, and the average V–N_{bpy} bond lengths are 2.233 Å. The N–O_{azoxy} (1.339 Å) and N–N (1.278 and 1.306 Å) bond lengths of the L_{ONO}^{2-} ligand are similar to those of the $\mathbf{3}^-$ ion. These features infer that the conversion of **1** to $\mathbf{1}^+$ is a metal-centred oxidation and that the $\mathbf{1}^+$ ion is a complex of the type $[(VO^{3+})(L_{ONO}^{2-})(bpy)]^+$.

Electronic Spectra

The electronic spectra of **1**, **2** and $\mathbf{3}^-NHEt_3^+$ in CH_2Cl_2 were recorded at 298 K. The spectra are illustrated in Figure 9, and the data are summarized in Table 6.

Complexes **1** and **2** exhibit absorption maxima at λ = 395 nm, whereas $\mathbf{3}^-NHEt_3^+$ absorbs at λ = 390 and 632 nm. The electronic spectra of $\mathbf{1}^+$, **3** and $\mathbf{3}^{2-}$ were recorded by spec-

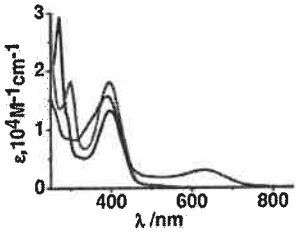

Figure 9. UV/Vis/NIR spectra of **1** (black), **2** (red) and **3**$^-$ (blue) in CH_2Cl_2 at 298 K.

Table 6. UV/Vis/NIR spectroscopic data of **1**–**3**$^-$ in CH_2Cl_2 at 298 K.

	λ_{max} [nm] (ε, 10^4 M^{-1} cm^{-1})
1	395 (1.32), 291 (1.26), 272 (2.92)
2	395 (2.72), 299 (2.71)
3$^-$ $NHEt_3^+$	632 (0.30), 390 (1.57), 340 (1.07), 296 (0.85), 261 (1.32)

troelectrochemical measurements, and the changes of the electronic spectra during the **1** → **1**$^+$, **3**$^-$ → **3** and **3**$^-$ → **3**$^{2-}$ conversions are depicted in Figure 10. One of the significant observations is that the intensity of the lower-energy absorption maximum of the **3**$^-$ ion at λ = 632 nm, which is absent for **1** and **2**, decreases gradually during the **3**$^-$ → **3** and **3**$^-$ → **3**$^{2-}$ conversions. The origin of this absorption is elucidated by time-dependent DFT (TD-DFT) calculations for the **3**$^-$ ion in CH_2Cl_2 by using the conductor-like polarizable continuum model (CPCM). The HOMO → LUMO (52 %; LUMO = lowest unoccupied molecular orbital) and HOMO–1 → LUMO (32 %) transitions are the dominant contribution to the lower-energy transition. The HOMO → LUMO transition is defined as a CSS → OSS perturbation transition. Thus, the λ_{max} at 632 nm is assigned to a CSS → OSS perturbation transition.[7b–7d] The calculated λ_{max} of **3**$^-$ at 403.5 nm is due to the L_{ONO}^{2-} → VO^{2+} ligand-to-metal charge-transfer (LMCT) transition. The stronger λ_{max} of **1** and **2** at 395 nm is assigned to L_{ONO}^{2-} → VO^{2+} charge-transfer transitions.

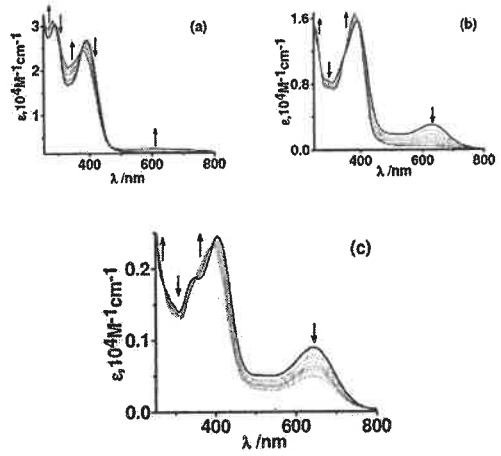

Figure 10. Changes to the UV/Vis absorption spectra during the conversions of (a) **1** → **1**$^+$, (b) **3**$^-$ → **3** and (c) **3**$^-$ → **3**$^{2-}$ recorded by spectroelectrochemical measurements.

Conclusions

Oxidovanadium(IV) complexes of 2,2-bipyridine (bpy), 1,10-phenanthronline (phen) and the *p*-nitro-*o*-iminobenzosemiquinone radical ($^{NO2}L_{ISQ}^{\bullet-}$) of types [(L_{ONO}^{2-})(VO)(bpy)] (**1**), [(L_{ONO}^{2-})(VO)(phen)] (**2**) and [(L_{ONO}^{2-})(VO)($^{NO2}L_{ISQ}^{\bullet-}$)]$^-$[$NHEt_3$]$^+$ (**3**$^-$ $NHEt_3^+$) with (–1, +4) state, as depicted in Table 1, are reported. The redox-innocent (*E*)-2-(3-hydroxy-3-phenyltriaz-1-en-1-yl)benzoic acid ($L_{ONO}H_2$) was used as a coligand. Complex **1** exhibits an anodic wave at 0.70 V owing to the VO^{3+}/VO^{2+} couple, which is not completely reversible, whereas the anodic and cathodic waves of the **3**$^-$ ion at 0.33 and –1.02 V (referenced to Fc^+/Fc couple) for the $^{NO2}L_{SQ}/^{NO2}L_{ISQ}^{\bullet-}$ and $^{NO2}L_{ISQ}^{\bullet-}/^{NO2}L_{AP}^{2-}$ couples are both reversible. DFT calculations established that the closed-shell-singlet (CSS) solution of **3**$^-$ is unstable owing to open-shell-singlet (OSS) perturbation, and the CSS → OSS charge-transfer transition appears at $\tilde{\nu}$ = 632 cm^{-1}. Complex **3** is defined as a hybrid of [(L_{ONO}^{2-})(VO^{2+})($^{NO2}L_{IQ}$)], (0, +4) and [(L_{ONO}^{2-})(VO^{3+})($^{NO2}L_{ISQ}^{\bullet-}$)], (–1, +5) states, whereas **3**$^{2-}$ is an oxidovanadium(IV) complex of type [(L_{ONO}^{2-})(VO^{2+})($^{NO2}L_{AP}^{2-}$)]$^{2-}$ (–2, +4).

Experimental Section

Materials and Physical Measurements: Reagent- or analytical-grade materials were obtained from commercial suppliers and used without further purification. Spectroscopic-grade solvents were used for spectroscopic and electrochemical measurements. The synthetic precursor $VO(acac)_2$[13] and the tridentate ligand (*E*)-2-(3-hydroxy-3-phenyltriaz-1-en-1-yl)benzoic acid ($L_{ONO}H_2$) were prepared by the reported procedures.[14] After the evaporation of the MeOH solvent of the samples under high vacuum, elemental analyses and spectral measurements were performed. The C, H and N contents of the compounds were obtained with a Perkin–Elmer 2400 series II elemental analyzer. The IR spectra of the samples were measured from $\tilde{\nu}$ = 4000 to 400 cm^{-1} with samples as KBr pellets at room temperature with a Perkin–Elmer Spectrum RX 1 FTIR spectrophotometer. The ^{1}H NMR spectra of samples in $CDCl_3$ were recorded with a Bruker DPX 300 MHz spectrometer with tetramethylsilane (TMS) as an internal reference. The ^{51}V NMR spectrum of **3**$^-$ $NHEt_3^+$ in $CDCl_3$ was recorded with a Bruker DPX 500 MHz spectrometer. The ESI mass spectra were recorded with a Micromass Q-TOF mass spectrometer. The electronic absorption spectra of solutions at 298 K were recorded with a Perkin–Elmer Lambda 25 spectrophotometer in the frequency range 1100–200 nm. A BASi Epsilon-EC electroanalytical instrument was used for the cyclic voltammetric experiments with CH_2Cl_2 solutions containing 0.2 M tetrabutylammonium hexafluorophosphate as the supporting electrolyte. A BASi platinum working electrode, a platinum auxiliary electrode and a Ag/AgCl reference electrode were used for the measurements. The redox potential data are referenced to the ferrocenium/ferrocene (Fc^+/Fc) couple. In all cases, the experiments were performed at multiple scan rates to analyze the reversibility of the electron-transfer waves. A BASi SEC-C thin-layer quartz glass spectroelectrochemical cell kit (light path length of 1 mm) with a platinum gauze working electrode and an SEC-C platinum counter electrode were used for the spectroelectrochemistry measurements. The X-band EPR spectra were recorded with a Magnettech GmbH MiniScope MS400 spectrometer (equipped with a TC H03 temperature controller), and the microwave frequency was measured with an FC400 frequency counter. The EPR spectra were simulated with the EasySpin software.

[(L_{ONO}^{2-})VO(bpy)] (1): To a solution of (*E*)-2-(3-hydroxy-3-phenyltriaz-1-en-1-yl)benzoic acid ($L_{ONO}H_2$; 257 mg, 1 mmol) in methanol (30 mL) at 325 K, $VO(acac)_2$ (262 mg, 1 mmol) and 2,2′-bipyridine (bpy) (156 mg, 1 mmol) were added, and the reaction mixture was heated under reflux for 30 min at 340 K. A deep red crystalline solid of **1** separated out. The solution mixture was cooled to 298 K, and the solid was collected by filtration. The residue was dried in air and collected for further analyses, yield 388 mg (ca. 81 % with respect to vanadium). Single crystals for X-ray diffraction study were prepared by the slow evaporation of a solution of **1** in CH_3OH in air at 298 K. MS (ESI+, CH_3OH): m/z = 479 $[M]^+$. $C_{23}H_{19}N_5O_5V$ (496.38, **1**·H_2O): calcd. C 55.65, H 3.86, N 14.11; found C 55.53, H 3.85, N 14.07. IR (KBr): $\tilde{\nu}$ = 1618 (s), 1605 (s), 1591 (s), 1475 (m), 1467 (m), 1442 (m), 1411 (s), 1342 (m), 1321 (m), 1223 (m), 1205 (m), 964 (s), 761 (s), 746 (m), 682 (m) cm^{-1}.

[(L_{ONO}^{2-})(VO)(phen)] (2): To a solution of $L_{ONO}H_2$ (257 mg, 1 mmol) in methanol (30 mL) at 325 K, $VO(acac)_2$ (262 mg, 1 mmol) and 1,10-phenanthroline (phen) (180 mg, 1 mmol) were added, and the reaction mixture was heated under reflux for 30 min at 340 K. A deep red crystalline solid of **2** separated out. The solution mixture was cooled to 298 K, and the solid was collected by filtration. The residue was dried in air and collected for further analyses, yield 412 mg (ca. 82 % with respect to vanadium). For X-ray diffraction study, single crystals of **2**·H_2O were prepared by the slow evaporation of a saturated solution of **2** in CH_3OH in air at 298 K. MS (ESI+, CH_3OH): m/z = 503 $[M]^+$. $C_{25}H_{19}N_5O_5V$ (520.40; **2**·H_2O): calcd. C 57.70, H 3.68, N 13.46; found C 57.56, H 3.67, N 13.42. IR (KBr): $\tilde{\nu}$ = 3413 (br), 1624 (s), 1603 (s), 1588 (m), 1407 (s), 1338 (m), 1326 (s), 1315 (m), 1220 (m), 1203 (m), 1045 (m), 966 (s), 757 (s), 725 (m), 684 (m) cm^{-1}.

[(L_{ONO}^{2-})(VO)($^{NO2}L_{ISQ}^{\bullet-}$)][$NHEt_3$] (3⁻ $NHEt_3^+$): To a solution of $L_{ONO}H_2$ (257 mg, 1 mmol) in methanol (30 mL) at 325 K, $VO(acac)_2$ (262 mg, 1 mmol) and *p*-nitro-*o*-aminophenol (144 mg, 1 mmol) were added. To this resulting solution, a few drops of triethylamine were added. The reaction mixture was evaporated slowly in air at 298 K, and deep green crystals of **3**⁻ $NHEt_3^+$ formed. The crystals were collected by filtration and dried in air for further analyses, yield 300 mg (ca. 52 % with respect to vanadium). MS (ESI–, CH_3OH): m/z = 474 $[\mathbf{3}]^-$. $C_{25}H_{29}N_6O_7V$ (576.48): calcd. C 52.09, H 5.07, N 14.58; found C 51.92, H 5.05, N 14.54. ^1H NMR ($CDCl_3$, 300 MHz, 300 K): δ = 13.97 (S, NH), 8.21 (d, 1 H), 7.97 (d, 1 H), 7.88 (d, 1 H), 7.81 (d, 1 H), 7.52 (d, 1 H), 7.43–7.34 (m, 4 H), 7.16 (t, 1 H), 6.36 (d, 1 H), 5.2 (s, 1 H) ppm. IR (KBr): $\tilde{\nu}$ = 3216 (br), 1599 (m), 1584 (m), 1573 (m), 1556 (m), 1489 (m), 1475 (s), 1467 (m), 1414 (m), 1360 (m), 1302 (s), 1280 (s), 1222 (m), 1078 (m), 944 (s), 683(m) cm^{-1}.

Single-Crystal X-ray Structure Determinations: Dark single crystals of **1**·H_2O, **2**·H_2O and **3**⁻ $NHEt_3^+$ were picked up with nylon loops and mounted in Bruker Kappa-CCD (100 K) and Bruker AXS D8 QUEST ECO (296 K) diffractometers equipped with a Mo-target rotating anode X-ray source and a graphite monochromator (Mo-K_α, λ = 0.71073 Å). The final cell constants were obtained from least-squares fits of all measured reflections. The intensity data were corrected for absorption from the intensities of redundant reflections. The structures were solved readily by direct methods and subsequent difference Fourier techniques. The crystallographic data of **1**, **2** and **3**⁻ $NHEt_3^+$ are listed in Table 7. SHELXS (Version 2013/1),[15a] SHELXT (version 2014/4),[15b] and SHELXL (version 2014/7)[15c] were used for the structure solution and refinement. All non-hydrogen atoms were refined anisotropically. Hydrogen atoms were placed at calculated positions and refined as riding atoms with isotropic displacement parameters.

Table 7. Crystallographic data for **1**·H_2O, **2**·H_2O and **3**⁻ $NHEt_3^+$.

	1·H_2O	**2**·H_2O	**3**⁻ $NHEt_3^+$
Formula	$C_{23}H_{19}N_5O_5V$	$C_{25}H_{19}N_5O_5V$	$C_{25}H_{29}N_6O_7V$
Fw	496.37	520.39	576.48
Crystal colour	red	orange	green
Crystal system	monoclinic	monoclinic	triclinic
Space group	*P*21/*c*	*P*21/*c*	*P*-1
a [Å]	9.5153(6)	8.898(2)	10.611(1)
b [Å]	27.829(2)	30.334(5)	11.642(1)
c [Å]	9.270(1)	9.308(2)	12.776(1)
α [°]	90	90.00	64.432(1)
β [°]	117.833(2)	116.515(3)	81.656(1)
γ [°]	90	90.00	78.017(1)
V [Å^3]	2170.8(2)	2248.1(8)	1390.00(8)
Z	4	4	2
T [K]	115(2)	100(2)	292(2)
2θ [°]	50.99	53.06	54.32
Density calcd. [g cm^{-3}]	1.519	1.538	1.377
Reflections collected	26757	47835	20016
Unique reflections	4035	4636	6116
Reflections [$I > 2\sigma(I)$]	3702	3592	5115
λ [Å]/μ [mm^{-1}]	0.71073/0.504	0.71073/0.491	0.71073/0.410
F(000)	1020	1068	600
R_1[a] [$I > 2\sigma(I)$]/GOF[b]	0.1021/1.244	0.0382/1.050	0.0585/1.046
R_1[a] (all data)	0.1121	0.0582	0.0705
wR_2[c] [$I > 2\sigma$ (*I*)]	0.2726	0.0781	0.1510
Parameters/restraints	307/0	331/2	359/0
Residual density [e Å^{-3}]	1.066	0.338	1.199

[a] $R_1 = \Sigma||F_o| - |F_c||/\Sigma|F_o|$. [b] GOF = $[\Sigma[w(F_o^2 - F_c^2)^2]/(n - p)]^{1/2}$. [c] $wR_2 = [\Sigma[w(F_o^2 - F_c^2)^2]/\Sigma[w(F_o^2)^2]]^{1/2}$; $w = 1/[\sigma^2(F_o^2) + (aP)^2 + bP]$, $P = (F_o^2 + 2F_c^2)/3$.

CCDC 1424292 (for **1**·H_2O), 1424293 (for **2**·H_2O) and 1424294 (for **3**⁻ $NHEt_3^+$) contain the supplementary crystallographic data for this paper. These data can be obtained free of charge from The Cambridge Crystallographic Data Centre.

Density Functional Theory (DFT) Calculations: All calculations reported in this article were performed with the Gaussian 03W[16] program package supported by GaussView 4.1. The DFT[17] and TD-DFT[18] calculations were performed at the level of the Becke three-parameter hybrid functional with the nonlocal correlation functional of Lee–Yang–Parr (B3LYP).[19] The gas-phase geometry of **3**⁻ was optimized with the Pulay direct inversion[20] in the iterative subspace (DIIS) with the "tight" convergent self-consistent field (SCF) procedure[21] with symmetry ignored and a singlet spin state. The analysis of the stability of the solution inferred that the closed-shell-singlet (CSS) solution of **3**⁻ was unstable. However, the stability of the broken-symmetry (1,1) solution, which converged to an M_s = 0 solution, indicated a diradical ground electronic state of the **3**⁻ ion. The gas-phase geometries of **3** and $\mathbf{3}^{2-}$ with doublet spin states were optimized with the B3LYP functional. All of the calculations were performed with a LANL2DZ basis set,[22] along with the corresponding effective core potential (ECP) for vanadium, a 6-31+G*-(d, p)[23] basis set for the C, O and N atoms, and 6-31G[24] for the H atoms. The 60 lowest singlet excitation energies of the optimized geometry of **3**⁻ with a closed-shell singlet spin state were calculated by the TD-DFT method. The nature of transitions was calculated by adding the probability of the same type among the molecular orbitals.

Acknowledgments

Financial support received from Department of Science and Technology (DST), New Delhi (grant number SR/S1/IC/0026/2012) and the Council of Scientific and Industrial Research

(CSIR), New Delhi [grant number 01(2699/12/EMR-II) and fellowships to S. M. and S. B.] is acknowledged.

Keywords: Oxidovanadium · Ligand effects · Radicals · Structure elucidation · Electronic structure

[1] a) G. Zampella, L. Bertini, L. De Gioia, *Chem. Commun.* **2014**, *50*, 304–307; b) M. R. Maurya, *Asian J. Chem.* **2012**, *24*, 5441–5446; c) V. Kraehmer, D. Rehder, *Dalton Trans.* **2012**, *41*, 5225–5234; d) M. R. Maurya, *J. Chem. Sci.* **2011**, *123*, 215–228; e) C. G. Werncke, C. Limberg, C. Knispel, R. Metzinger, B. Braun, *Chem. Eur. J.* **2011**, *17*, 2931–2938; f) L. F. Pacios, O. Gálvez, *J. Chem. Theory Comput.* **2010**, *6*, 1738–1752; g) D. Rehder, *Chem. Unserer Zeit* **2010**, *44*, 322–331; h) K. R. Geethalakshmi, M. P. Waller, W. Thiel, M. Bühl, *J. Phys. Chem. B* **2009**, *113*, 4456–4465; i) C. J. Schneider, G. Zampella, L. DeGioa, V. L. Pecoraro, *ACS Symposium Series*, vol. 974: *Vanadium: The Versatile Metal* (Eds.: K. Kustin, J. C. Pessoa, D. C. Crans), American Chemical Society, Washington, DC, **2009**, chapter 12, p. 148–162; j) M. Mba, M. Pontini, S. Lovat, C. Zonta, G. Bernardinelli, P. E. Kündig, G. Licini, *Inorg. Chem.* **2008**, *47*, 8616–8618; k) M. R. Maurya, *J. Chem. Sci.* **2006**, *118*, 503; l) G. Zampella, P. Fantucci, V. L. Pecoraro, L. De Gioia, *Inorg. Chem.* **2006**, *45*, 7133–7143.

[2] a) A. W. Fay, M. A. Blank, C. C. Lee, Y. Hu, K. O. Hodgson, B. Hedman, M. W. Ribbe, *J. Am. Chem. Soc.* **2010**, *132*, 12612–12618; b) S. Ye, F. Neese, A. Ozarowski, D. Smirnov, J. Krzystek, J. Telser, J.-H. Liao, C.-H. Hung, W.-C. Chu, Y.-F. Tsai, R.-C. Wang, K.-Y. Chen, H.-F. Hsu, *Inorg. Chem.* **2010**, *49*, 977–988; c) K. Fisher, M. J. Dilworth, W. E. Newton, *Biochemistry* **2006**, *45*, 4190–4198; d) G. N. George, C. L. Coyle, B. J. Hales, S. P. Cramer, *J. Am. Chem. Soc.* **1988**, *110*, 4057–4059; e) D. Rehder, *Inorg. Chem. Commun.* **2003**, *6*, 604–617; f) R. R. Eady, *Coord. Chem. Rev.* **2003**, *237*, 23–30; g) D. J. Rehder, *J. Inorg. Biochem.* **2000**, *80*, 133–136.

[3] a) A. Levina, A. I. McLeod, S. J. Gasparini, A. Nguyen, W. G. M. De Silva, J. B. Aitken, H. H. Harris, C. Glover, B. Johannessen, P. A. Lay, *Inorg. Chem.* **2015**, *54*, 7753–7766; b) A. Levina, A. I. McLeod, A. Pulte, J. B. Aitken, P. A. Lay, *Inorg. Chem.* **2015**, *54*, 6707–6718; c) Y. Yoshikawa, H. Sakurai, D. C. Crans, G. Micera, E. Garribba, *Dalton Trans.* **2014**, *43*, 6965–6972; d) D. Sanna, M. Serra, G. Micera, E. Garribba, *Inorg. Chem.* **2014**, *53*, 1449–1464; e) D. Sanna, M. Serra, G. Micera, E. Garribba, *Inorg. Chim. Acta* **2014**, *420*, 75–84; f) D. Sanna, G. Micera, E. Garribba, *Inorg. Chem.* **2013**, *52*, 11975–11985; g) P. W. Winter, A. Al-Qatati, A. L. Wolf-Ringwall, S. Schoeberl, P. B. Chatterjee, B. G. Barisas, D. A. Roess, D. C. Crans, *Dalton Trans.* **2012**, *41*, 6419–6430.

[4] a) C. C. McLauchlan, B. J. Peters, G. R. Willsky, D. C. Crans, *Coord. Chem. Rev.* **2015**, *301–302*, 163; b) N. Butenko, J. P. Pinheiro, J. P. Da Silva, A. I. Tomaz, I. Correia, V. Ribeiro, J. C. Pessoa, I. Cavaco, *J. Inorg. Biochem.* **2015**, *147*, 165; c) I. S. Lombardo, S. Alvarez, C. C. McLauchlan, D. C. Crans, *J. Inorg. Biochem.* **2015**, *147*, 153–164; d) P. Zabierowski, J. Szklarzewicz, R. Gryboś, B. Modryl, W. Nitek, *Dalton Trans.* **2014**, **43**, *45*, 17044; e) V. I. Kuznetsov, A. N. Alexandrova, A. C. Hengge, *J. Am. Chem. Soc.* **2012**, *134*, 14298–14301; f) D. R. Davies, W. G. J. Hol, *FEBS Lett.* **2004**, *577*, 315–321.

[5] a) J. C. Pessoa, S. Etcheverry, D. Gambino, *Coord. Chem. Rev.* **2015**, *301–302*, 24–48; b) D. Rehder, *Future Med. Chem.* **2012**, *4*, 1823–1837; c) D. C. Crans, T. J. Meade, *Inorg. Chem.* **2013**, *52*, 12181–12183; d) D. C. Crans, K. A. Woll, K. Prusinskas, M. D. Johnson, E. Norkus, *Inorg. Chem.* **2013**, *52*, 12262–12275.

[6] M. R. Maurya, *Coord. Chem. Rev.* **2003**, *237*, 163–181.

[7] a) M. Stylianou, C. Drouza, J. Giapintzakis, G. I. Athanasopoulos, A. D. Keramidas, *Inorg. Chem.* **2015**, *54*, 7218–7229; b) S. Kundu, S. Maity, T. Weyhermüller, P. Ghosh, *Inorg. Chem.* **2013**, *52*, 7417–7430; c) S. Kundu, S. Maity, A. N. Maity, S.-C. Ke, P. Ghosh, *Inorg. Chem.* **2013**, *52*, 7417–7430; d) A. S. Roy, P. Saha, N. D. Adhikary, P. Ghosh, *Inorg. Chem.* **2011**, *50*, 2488–2500; e) C. Drouza, A. D. Keramidas, *Inorg. Chem.* **2008**, *47*, 7211–7224; f) C. Drouza, V. Tolis, V. Gramlich, C. Raptopoulou, A. Terzis, M. P. Sigalas, T. A. Kabanos, A. D. Keramidas, *Chem. Commun.* **2002**, 2786–2787.

[8] a) C. Wolff, A. Gottschlich, J. England, K. Wieghardt, W. Saak, D. Haase, R. Beckhaus, *Inorg. Chem.* **2015**, *54*, 4811–4820; b) C. C. Scarborough, K. Wieghardt, *Inorg. Chem.* **2011**, *50*, 9773–9793; c) E. Gore-Randall, M. Irwin, M. S. Denning, J. M. Goicoecchea, *Inorg. Chem.* **2009**, *48*, 8304.

[9] a) W. Kaim, *Inorg. Chem.* **2011**, *50*, 9752–9765; b) W. Kaim, B. Schwederski, *Coord. Chem. Rev.* **2010**, *254*, 1580–1588; c) A. I. Poddel'sky, V. K. Cherkasov, G. A. Abakumov, *Coord. Chem. Rev.* **2009**, *253*, 291–324; d) P. Chaudhuri, C. N. Verani, E. Bill, E. Bothe, T. Weyhermüller, K. Wieghardt, *J. Am. Chem. Soc.* **2001**, *123*, 2213–2223; e) H. Chun, E. Bill, T. Weyhermüller, K. Wieghardt, *Angew. Chem. Int. Ed.* **2001**, *40*, 2489–2492; *Angew. Chem.* **2001**, *113*, 2552.

[10] a) J. Pranczk, D. Jacewicz, D. Wyrzykowski, A. Wojtczak, A. Tesmar, L. Chmurzynski, *Eur. J. Inorg. Chem.* **2015**, 3343–3349; b) S. Kodama, N. Taya, Y. Ishii, *Inorg. Chem.* **2014**, *53*, 2754–2756; c) R. Takjoo, J. T. Mague, A. Akbari, S. Y. Ebrahimipour, *J. Coord. Chem.* **2013**, *66*, 2852–2862; d) B. Balaji, B. Banik, P. K. Sasmal, B. Maity, R. Majumdar, R. R. Dighe, A. R. Chakravarty, *Eur. J. Inorg. Chem.* **2012**, 126–135; e) R. Dong-xue, C. Yunzhu, C. Chen, X. Yong-heng, *Chem. Res. Chin. Univ.* **2012**, *28*, 768–774; f) M. Sutradhar, T. Roy Barman, G. Mukherjee, M. G. B. Drew, S. Ghosh, *Inorg. Chim. Acta* **2010**, *363*, 3376–3383; g) H.-Y. Zhao, Y.-H. Xing, Y.-Z. Cao, Z.-P. Li, D.-M. Wei, X.-Q. Zeng, M.-F. Ge, *J. Mol. Struct.* **2009**, *938*, 54–64; h) G. D. Triantafillou, E. I. Tolis, A. Terzis, Y. Deligiannakis, C. P. Raptopoulou, M. P. Sigalas, T. A. Kabanos, *Inorg. Chem.* **2004**, *43*, 79–91; i) J. Chakravarty, S. Dutta, S. K. Chandra, P. Basu, A. Chakravorty, *Inorg. Chem.* **1993**, *32*, 4249–4255.

[11] a) D. Herebian, K. Wieghardt, F. Neese, *J. Am. Chem. Soc.* **2003**, *125*, 10997–11005; b) M. M. Khusniyarov, T. Weyhermüller, E. Bill, K. Wieghardt, *J. Am. Chem. Soc.* **2009**, *131*, 1208–1221; c) S. Mukherjee, T. Weyhermüller, E. Bill, K. Wieghardt, P. Chaudhuri, *Inorg. Chem.* **2005**, *44*, 7099–7108; d) S. Kokatam, T. Weyhermüller, E. Bothe, P. Chaudhuri, K. Wieghardt, *Inorg. Chem.* **2005**, *44*, 3709–3717; e) K. S. Min, T. Weyhermüller, E. Bothe, K. Wieghardt, *Inorg. Chem.* **2004**, *43*, 2922–2931.

[12] P. B. Chatterjee, O. G. Zapata, L. L. Quinn, G. Hou, H. Hamaed, R. W. Schurko, T. Polenova, D. C. Crans, *Inorg. Chem.* **2011**, *50*, 9794–9803.

[13] R. A. Rowe, M. M. Jones, *Inorg. Synth.* **1957**, *5*, 113–115.

[14] S. C. Saha, S. Maji, *Ind. J. Chem. A* **1990**, *29A*, 573–576.

[15] a) G. M. Sheldrick, *SHELXS Version 2013/1*, University of Göttingen, Germany, **2013**; b) G. M. Sheldrick, *Acta Crystallogr., Sect. A* **2015**, *71*, 3–8; c) G. M. Sheldrick, *Acta Crystallogr., Sect. C* **2015**, *71*, 3–8.

[16] M. J. Frisch, G. W. Trucks, H. B. Schlegel, G. E. Scuseria, M. A. Robb, J. R. Cheeseman, J. A. Montgomery Jr., T. Vreven, K. N. Kudin, J. C. Burant, J. M. Millam, S. S. Iyengar, J. Tomasi, V. Barone, B. Mennucci, M. Cossi, G. Scalmani, N. Rega, G. A. Petersson, H. Nakatsuji, M. Hada, M. Ehara, K. Toyota, R. Fukuda, J. Hasegawa, M. Ishida, T. Nakajima, Y. Honda, O. Kitao, H. Nakai, M. Klene, X. Li, J. E. Knox, H. P. Hratchian, J. B. Cross, V. Bakken, C. Adamo, J. Jaramillo, R. Gomperts, R. E. Stratmann, O. Yazyev, J. A. Austin, R. Cammi, C. Pomelli, J. W. Ochterski, P. Y. Ayala, K. Morokuma, G. A. Voth, P. Salvador, J. J. Dannenberg, V. G. Zakrzewski, S. Dapprich, A. D. Daniels, M. C. Strain, O. Farkas, D. K. Malick, A. D. Rabuck, K. Raghavachari, J. B. Foresman, J. V. Ortiz, Q. Cui, A. G. Baboul, S. Clifford, J. Cioslowski, B. B. Stefanov, G. Liu, A. Liashenko, P. Piskorz, I. Komaromi, R. L. Martin, D. J. Fox, T. Keith, M. A. Al-Laham, C. Y. Peng, A. Nanayakkara, M. Challacombe, P. M. W. Gill, B. Johnson, W. Chen, M. W. Wong, C. Gonzalez, J. A. Pople, *Gaussian 03*, revision E.01, Gaussian, Inc., Wallingford, CT, **2004**.

[17] a) R. G. Parr, W. Yang, *Density Functional Theory of Atoms and Molecules*, Oxford University Press, Oxford, UK, **1989**; b) D. R. Salahub, M. C. Zerner (Eds.), *ACS Symposium Series*, vol. 394: *The Challenge of d and f Electrons*, American Chemical Society, Washington, DC, **1989**; c) W. Kohn, L. Sham, *J. Phys. Rev.* **1965**, *140*, A1133–A1138; d) P. Hohenberg, W. Kohn, *Phys. Rev.* **1964**, *136*, B864–B871.

[18] a) R. E. Stratmann, G. E. Scuseria, M. Frisch, *J. Chem. Phys.* **1998**, *109*, 8218–8224; b) M. E. Casida, C. Jamoroski, K. C. Casida, D. R. Salahub, *J. Chem. Phys.* **1998**, *108*, 4439–4449; c) R. Bauernschmitt, M. Haser, O. Treutler, R. Ahlrichs, *Chem. Phys. Lett.* **1996**, *256*, 454–464.

[19] a) A. D. Becke, *J. Chem. Phys.* **1993**, *98*, 5648–5652; b) B. Miehlich, A. Savin, H. Stoll, H. Preuss, *Chem. Phys. Lett.* **1989**, *157*, 200–205; c) C. Lee, W. Yang, R. G. Parr, *Phys. Rev. B* **1988**, *37*, 785–789.

[20] P. J. Pulay, *Comput. Chem.* **1982**, *3*, 556–560.

[21] H. B. Schlegel, J. J. McDouall, in: *Computational Advances in Organic Chemistry* (Eds.: C. Ogretir, I. G. Csizmadia), Kluwer Academic, Dordrecht, The Netherlands, **1991**, p. 167–185.

[22] a) P. J. Hay, W. R. Wadt, *J. Chem. Phys.* **1985**, *82*, 270–283; b) W. R. Wadt, P. J. Hay, *J. Chem. Phys.* **1985**, *82*, 284–298; c) P. J. Hayand, W. R. Wadt, *J. Chem. Phys.* **1985**, *82*, 299–310.
[23] W. J. Hehre, R. Ditchfield, J. A. Pople, *J. Chem. Phys.* **1972**, *56*, 2257–2261.
[24] a) V. A. Rassolov, M. A. Ratner, J. A. Pople, P. C. Redfern, L. A. Curtiss, *J. Comput. Chem.* **2001**, *22*, 976–984; b) M. M. Francl, W. J. Pietro, W. J. Hehre, J. S. Binkley, D. J. DeFrees, J. A. Pople, M. S. Gordon, *J. Chem. Phys.* **1982**, *77*, 3654–3665; c) P. C. Hariharan, J. A. Pople, *Mol. Phys.* **1974**, *27*, 209–214; d) P. C. Hariharan, J. A. Pople, *Theo. Chim. Acta* **1973**, *28*, 213–222; e) W. J. Hehre, R. Ditchfield, J. A. Pople, *J. Chem. Phys.* **1972**, *56*, 2257–2261.

Received: October 30, 2015
Published Online: January 4, 2016